The Astrophysical Journal, 785:41 (9pp), 2014 April 10 doi:10.1088/0004-637X/785/1/41

OBSERVATIONAL EVIDENCE OF DUST EVOLUTION IN GALACTIC EXTINCTION CURVES

Cesare Cecchi-Pestellini[1], Silvia Casu[2], Giacomo Mulas[2], and Alberto Zonca[3]
[1] INAF-Osservatorio Astronomico di Palermo, P.zza Parlamento 1, I-90134 Palermo, Italy; cecchi-pestellini@astropa.unipa.it
[2] INAF-Osservatorio Astronomico di Cagliari, Via della Scienza, I-09047 Selargius (CA), Italy; silvia@oa-cagliari.inaf.it, gmulas@oa-cagliari.inaf.it
[3] Dipartimento di Fisica, Università di Cagliari, Strada Prov.le Monserrato-Sestu Km 0.700, I-09042 Monserrato (CA), Italy; azonca@oa-cagliari.inaf.it
Received 2013 October 25; accepted 2013 December 20; published 2014 March 25

ABSTRACT

Although structural and optical properties of hydrogenated amorphous carbons are known to respond to varying physical conditions, most conventional extinction models are basically curve fits with modest predictive power. We compare an evolutionary model of the physical properties of carbonaceous grain mantles with their determination by homogeneously fitting observationally derived Galactic extinction curves with the same physically well-defined dust model. We find that a large sample of observed Galactic extinction curves are compatible with the evolutionary scenario underlying such a model, requiring physical conditions fully consistent with standard density, temperature, radiation field intensity, and average age of diffuse interstellar clouds. Hence, through the study of interstellar extinction we may, in principle, understand the evolutionary history of the diffuse interstellar clouds.

Key words: dust, extinction – evolution – ISM: clouds

Online-only material: color figures

1. INTRODUCTION

Over the last half century, it has become increasingly evident that interstellar dust, which lost the role of nuisance, is a crucial component of the Milky Way and other galaxies. Despite the many very important roles played by cosmic dust in astronomy, a similar change of perspective has not been realized in its modeling. Dust properties are known to vary and clearly grains are not immutable. Still, most conventional extinction models are basically curve fits with modest, if any, predictive power.

The life cycle of cosmic matter is closely related to the cycle of the interstellar medium and our Galaxy. During their lifetimes, dust grains are affected by many processes as they transform from diffuse to dense clouds or during the collapse of dense molecular clouds. These processes may destroy the grains, violently, by shattering, or more gently, by sputtering, determining, e.g., their size distribution. The wide variations of InterStellar Extinction Curves (ISECs) in the Milky Way (Fitzpatrick & Massa 2007) and other galaxies (e.g., Maíz Apellániz & Rubio 2012) may thus reflect the intrinsic variability expected from an interstellar medium with a wide range in physical properties and grain-processing histories. Since such processes are random in nature, it may appear difficult to reconcile the remarkable variations of the interstellar extinction profiles within an unified scheme. Still, ISECs have been shown to be characterized by a very small number of regulatory parameters (e.g., Valencic et al. 2004).

The models originating with Jones et al. (1990) and pursued in detail by Cecchi-Pestellini & Williams (1998) and Cecchi-Pestellini et al. (2010) claim that the physical and chemical nature of grains—and in particular their optical properties—respond to the local physical conditions in the diffuse interstellar medium and evolve in time. Carbon in the H-rich diffuse interstellar gas is deposited on silicate dust grains initially in the form of sp^3 hydrogenated amorphous carbon. The interstellar radiation field then progressively processes this material into an H-poor sp^2 carbon on a timescale expected to be less than or about one million years. The reverse re-hydrogenation reaction also takes place, driven by accretion of hot hydrogen atoms, so that the net rate of graphitization results from the competition between the two opposite processes, depending on local conditions. The deposition time is on the order of a few million years for typical number densities, while removal of the carbon by relatively low-velocity shocks is probably on the same timescale. In this scenario, therefore, the extinction caused by such grains varies with time. We here aim to show that the changing nature of the ISECs may be understood, within the framework of such a model, as a manifestation of the evolution of carbon in the interstellar medium, which in turn depends mainly on the relative abundances of sp^2 and sp^3 bonding sites (e.g., Chiar et al. 2013). Our conclusions are based on the global characterization of the Galactic extinction (although limited to just 2 kpc around the Sun's location in the Milky Way) in terms of the physical parameters of a well-defined dust model performed by Mulas et al. (2013).

The extinction model adopted in Mulas et al. (2013), which is just an extinction model, assumes a parameterized physical structure of dust particles, together with their size distribution, and determines the set of parameters that best match each observed extinction curve. The interpretation of the obtained parameter values requires an underlying chemical and physical description of the properties of dust materials and their response to the local physical conditions along specific lines of sight. In light of such a physical interpretation, each set of fitted parameters is the product of the history of a given dust population and can be used to tell its tale. We derive here a model of the evolution of dust particles and compare its predictions with the results of Mulas et al. (2013). It is well known that changes in the optical properties of hydrogenated amorphous carbon are driven by ultraviolet irradiation and thermal annealing processes (Iida et al. 1984; Robertson 1991). Such events occur in space mainly in response to ultraviolet radiation fields (Jones 2012a). We model the process considering gas-phase carbon progressively deposited on silicate cores. Initially, mantles are assumed to be H-rich amorphous carbon. This assumption is the natural consequence of deposition occurring in an atomic H environment. Simultaneous ultraviolet processing of this material forms two distinct concentric shells,

connected by a fuzzy transition layer to account for carbon mantle formation by successive deposition of atoms (see Iatì et al. 2008 for details). If the annealing timescale is much shorter than deposition, or when the available gas-phase carbon is exhausted, the outer sp^3 layer becomes vanishingly thin. If, conversely, the annealing timescale is much longer than deposition, the H-rich carbon mantle will become optically thick in the ultraviolet, so that sp^3 layers deeper than approximately 20 nm will be shielded and will not be further processed (Jones 2012b). Although simplified, this approach allows one to follow in fair detail the compositional and structural evolution of dust carbonaceous materials and their impact on the optical properties of dust.

Recently, Jones et al. (2013) put forward a dust model in which aliphatic carbon deposition is assumed to occur in dense clouds, whereas processing occurs in diffuse clouds. Moreover, they include a population of large carbonaceous grains, initially H rich before processing. For the thick aliphatic mantles they assume to be deposited in dense clouds, and even more so for big carbonaceous grains, self-shielding is an issue and under their assumptions it is reasonable to expect more processed material in outer layers and less processed material inside. Actually, one would expect even an onion structure, when more cycles accumulate. If it is assumed that in diffuse interstellar regions photo-processing rates are fast enough, the outer layer of freshly deposited, still unprocessed, aliphatic material would be so thin as to be negligible.

In the present evolutionary model of mantle accretion and processing, which we consider to occur in the diffuse-to-translucent interstellar medium (i.e., not in molecular dense clouds), we allow for an ample range of densities and radiation field intensities and quantitatively follow the time evolution of grain mantles, using a time-dependent gas-phase chemistry model to determine the time-dependent deposition rate. This is a significant difference from the Jones et al. (2013) model, in which mantle thickness and the fraction of processed versus unprocessed carbon are not allowed to vary but stem from assumptions.

The purpose of this work is to give a physical interpretation of the observed visible-ultraviolet extinction curves in Fitzpatrick & Massa (2007), as fit by Mulas et al. (2013). All of these lines of sight have a relatively low extinction, which is an obvious observational bias due to the availability of ultraviolet observations. This observational bias, however, translates in a physical one: each low-extinction line of sight in the solar vicinity is more sensibly representable by a single set of dust model parameters. It would be conceptually wrong and physically meaningless to try to use such a simplistic representation to interpret any observations of lines of sight with a much larger extinction, unless there are strong reasons to believe that they are specifically dominated by a single, remarkably uniform set of conditions across the whole line of sight. Reality is usually more complicated, as in heavily reddened lines of sight there is typically a superposition of numerous interstellar clouds with more or less widely different physical conditions.

In Section 2, we present a brief description of the adopted model for the evolution of dust structural and optical properties and we examine the general properties of the solutions of its differential equations. Section 3 contains an outline of the dust models used by Mulas et al. (2013) to fit a large sample of Galactic ISECs, yielding observational estimates of the same dust mantle parameters modeled in the previous section. The results of the comparison between model and observations and their implications for the Galactic dust evolution are presented in Section 4, while the last section contains our conclusions.

2. THE MODEL OF INTERSTELLAR DUST EVOLUTION

2.1. Outline

Initially, the silicate cores are assumed to be bare. Then, carbon is deposited kinetically from the gas with a rate depending on the gas density and temperature. The resulting solid carbon layer is assumed, at deposition, to be hydrogen rich and sp^3 bonded. Ultraviolet irradiation of the H-rich polymeric carbon will reduce the H content and lower the bandgap energy, making the material appear more graphitic, increasing the absorption of such material in the visible and causing luminescence in the infrared. Conversely, the exposure of graphitic carbon to hot H atoms can reverse the process: the carbon becomes richer in hydrogen, the bandgap increases, the material absorbs more strongly in the ultraviolet, and luminescences in the visible with high efficiency. Strong ultraviolet processing (e.g., in photon-dominated regions) and sufficiently elevated temperatures (e.g., during a shock) will remove the carbon mantles entirely in the form of carbon atoms and ions, carbon molecules and radicals, and polycyclic aromatic hydrocarbons (PAHs).

Such a cycle of carbon in and out of dust is described by a set of ordinary differential equations that follow the evolution in time of the available carbon fraction $x_{\rm C}$, the deposited polymeric sp^3 carbon fraction x_{sp^3}, and its radiation-annealed sp^2 counterpart x_{sp^2}:

$$\begin{cases} \dfrac{dx_{\rm C}}{dt} = -\left(A + k_{\rm chem}\right) x_{\rm C} \\ \dfrac{dx_{sp^3}}{dt} = A x_{\rm C} - t_{\rm pd}^{-1} x_{sp^3} + k_{\rm H^\star} x_{sp^2} \\ \dfrac{dx_{sp^2}}{dt} = t_{\rm pd}^{-1} x_{sp^3} - k_{\rm H^\star} x_{sp^2} \end{cases} \tag{1}$$

together with the normalization condition $x_{\rm C} + x_{sp^3} + x_{sp^2} + x_{\rm gp} = 1$, $x_{\rm gp}$ being the fractional abundance of gas-phase carbon. The system of Equation (1) is coupled with an additional equation for the evolution of carbon column density of the material composing the mantle $N_{\rm C} = \delta_{\rm C} \times w$. Since both mantle density and thickness are functions of time, we derive the mantle width evolution as follows

$$\begin{aligned} \frac{dN_{\rm C}}{dt} &= w\frac{d\delta_{\rm C}}{dt} + \delta_{\rm C}\frac{dw}{dt} = D\, x_{\rm C} \\ \frac{dw}{dt} &= \left(\frac{D}{\delta_{\rm C}}\right) x_{\rm C} - \left(\frac{w}{\delta_{\rm C}}\right)\frac{d\delta_{\rm C}}{dt}. \end{aligned} \tag{2}$$

Equations (1) and (2) are linked to a set of chemical rate equations describing gas-phase chemistry. In Equation (1) $A = \xi\, v_{\rm C}\, (\langle\sigma_d n_d\rangle/[{\rm H}])\, n_{\rm H}$, where ξ is the carbon sticking coefficient, $v_{\rm C} = \sqrt{8kT_{\rm k}/\pi m_{\rm C}}$ is the C grain relative thermal velocity, $\langle\sigma_d n_d\rangle/[{\rm H}]$ is the C dust collision rate per nucleon averaged over the dust size distribution, and $n_{\rm H}$ is the total number density of H nuclei. $k_{\rm chem}$ is a cumulative chemical rate for the formation of carbon-bearing gas-phase species such as CO, $k_{\rm H^\star}$ is the $sp^2 \rightarrow sp^3$ conversion rate via hot atomic H insertion in the aromatic matrix, and

$$t_{\rm pd}^{-1} = \int \sigma_{\rm pd}(\nu) I_{\rm UV}(\nu,\Omega) d\nu\, d\Omega \tag{3}$$

is the photo-darkening rate and $\sigma_{\rm pd}(\nu)$ and $I_{\rm UV}$ are the photo-darkening cross section (e.g., Mennella et al. 2001) and the interstellar ultraviolet radiation field, respectively. Because of irradiation, in carbon materials exposed to above- and near-bandgap radiation the absorption coefficient over a broad range of frequencies increases. The amount of increase depends on the wavelength and the intensity of the inducing radiation and the duration of the exposure, leading to a shift of the optical absorption edge to lower energy and an increase in the band-tail absorption. The physical and chemical transformation is complex, involving selective photodissociation of chemical bonds, selective sputtering that reduces the relative H, N, and O content, restructuring of chemical bonds to form increasingly large aromatic platelets (see, e.g., Jones 2012a, 2012b). However, the net apparent effect is a change in color of the processed carbonaceous material, with a progressive darkening, i.e., from transparent to "yellow stuff" and to "brown stuff" (Greenberg 1984). In the simplified description adopted here, in which we consider only the extreme cases of sp^3 and sp^2 material, $t_{\rm pd}$ quantitatively determines the timescale for ultraviolet irradiation to transform the former into the latter.

Finally, in Equation (2), the coefficient $D = v_{\rm C} m_{\rm C} \mathcal{A}_{\rm C}(1 - f_{\rm PAH}) n_{\rm H}$ is the mass accretion rate over a spherical surface, derived assuming grains of different sizes accrete mantles with the same thickness (Whittet 2003). According to this definition, $\mathcal{A}_{\rm C}$ is the total carbon elemental abundance and $f_{\rm PAH}$ is the fraction of carbon in PAHs. Since the two forms of carbon, amorphous and polymeric, have different mass densities, $\delta_{sp^2} = 2.26$ g cm^{-3} (graphite) and $\delta_{sp^3} = 0.901$ g cm^3 (polyethylene), respectively, the mantle density $\delta_{\rm C}$ is time-dependent (see the second term in the right-hand side of Equation (2). We do not consider PAH accretion onto the dust surface, which is likely to occur but at a marginal rate with respect to atomic C collisions.

The term $k_{\rm chem}$ summarizes a simple chemical network constructed from 139 species consisting of the elements H, He, C, O, N, and S. With the exception of carbon, the concentrations of the elements relative to H, equal to 10^5 (He), 200 (O), 50 (N), and 3 (S) ppm, refer exclusively to the abundances in the gas phase. The total concentration of C, in both gas and solid phases, is $\mathcal{A}_{\rm C} = 225$ ppm (Snow & Witt 1996). Estimating the absolute abundances of the elements in the interstellar medium is a difficult task and here we use a conservative choice. We note that the increase, or decrease, of the available gas-phase carbon is not linearly reflected in the mantle accretion rate, which depends on the product of $\mathcal{A}_{\rm C}$ and the carbon sticking coefficient ξ, with this latter quantity determined by the observationally inferred CO concentrations.

We select from the UDFA data file (Woodall et al. 2007) all the reactions that couple the species, for a total number of ~2000 reactions. The cosmic ray ionization rate ζ is four times the standard UDFA value, i.e., $\zeta = 5 \times 10^{-17}$ s^{-1}. The chemical abundances have been checked for consistency, but exploited only to derive the value of the sticking coefficient consistent with the presence of the observationally determined abundance of CO in molecular clouds, $\xi \lesssim 0.1$. The chemical model is described elsewhere (Casu et al. 2001). The model consists of a time-dependent, photon-dominated region code, describing a two-sided illuminated cloud with $A_V = 1$.

Equations (1) and (2) should be supplemented with suitable terms describing mantle sputtering or evaporation in shocks or other destructive events (e.g., Jones et al. 1996). However, here we follow dust and chemistry evolution one cycle at a time. We also do not explicitly include rehydrogenation and set $k_{\rm H^\star} = 0$. Starting with bare silicate cores, the initial conditions at $t = 0$ are $x_{\rm C} = 1$, $x_{\rm gp} = 0$, $w = 0$, and $x_{sp^3} = x_{sp^2} = 0$. Destructive events are taken into account by abruptly removing part of the mantle, leaving a remnant with an arbitrary sp^2/sp^3 ratio and resuming the evolution from these new initial conditions.

2.2. Properties of the Solutions

Equations (1) and (2) can be recast more compactly. First, we decouple gas-phase chemistry from carbon accretion on dust surfaces by subtracting from the total carbon abundance the gas-phase component and setting $k_{\rm chem} = 0$. Then, scaling the integration variable to $ds = T_{\rm k}^{1/2} n_{\rm H} dt$ and incorporating into the newly defined carbon elemental abundance $\hat{\mathcal{A}}_{\rm C}$ the factor $(1 - f_{\rm PAH})$, we obtain

$$\begin{cases} \dfrac{dx_{\rm C}}{ds} = -\hat{A} x_{\rm C} \\ \dfrac{dx_{sp^3}}{ds} = \hat{A} x_{\rm C} - s_{\rm pd}^{-1} x_{sp^3} \\ \dfrac{dx_{sp^2}}{ds} = s_{\rm pd}^{-1} x_{sp^3} \\ \dfrac{dw}{ds} = \left(\dfrac{\hat{D}}{\delta_{\rm C}}\right) x_{\rm C} - \left(\dfrac{w}{\delta_{\rm C}}\right) \dfrac{d\delta_{\rm C}}{ds}, \end{cases} \tag{4}$$

where $x_{\rm C} + x_{sp^3} + x_{sp^2} = 1$, $\hat{A} = (8k/\pi m_{\rm C})^{1/2} (\langle \sigma_d n_d \rangle / [{\rm H}])$, $\hat{D} = (8 k m_{\rm C}/\pi)^{1/2} \hat{\mathcal{A}}_{\rm C}$, and $s_{\rm pd} = (T_{\rm k}^{1/2} n_{\rm H}/\chi) t_{\rm pd}$ is the scaled photo-darkening time, with χ being the increase of the interstellar ultraviolet radiation field $I_{\rm UV}$ with respect to the interstellar standard value. We have, thus, a one-parameter system of differential equations, which can be easily integrated numerically. Solutions starting from the same initial conditions, but with different $s_{\rm pd}$ values, have no other points in common but the starting point and the asymptotic limit ($s \to \infty$).

This is apparent from Figure 1, which shows in each panel the evolutionary tracks resulting from a set of initial conditions. We plot the quantity $f_{sp^2} = \delta_{sp^2} x_{sp^2} / (\delta_{sp^2} x_{sp^2} + \delta_{sp^3} x_{sp^3})$, a function of the parameters of the present evolutionary model, to make possible a direct comparison with the results of the ISEC fitting procedure (see Section 3). We chose four initial conditions and for each one we produced curves corresponding to a grid of sensible values of the only free parameter $s_{\rm pd}$. From the evolutionary point of view, the curves in top left panel of Figure 1 represent the initial evolution from pristine, naked silicate grains, i.e., the very first cycle in the life of an interstellar grain. The other cases represent the evolution of grain mantles restarting after a mantle-shattering event. In such a case, a small layer of residual mantle is left, which may have been rehydrogenated to some extent by impinging hot H atoms in the same event. In the plot, we also show the iso-s curves, relating different evolutionary tracks at the same values of the evolution parameter s. Curves in the same panel never intersect and are thus invertible for the given initial conditions. Inverting them produces a (scaled) evolutionary time, $s_{\rm ev}$, derived from the knowledge of, e.g., x_{sp^2} and w for any value of $s_{\rm pd}$.

We consider $\hat{\mathcal{A}}_{\rm C}$ to be constant along different lines of sight. This is not an extreme approximation as $\hat{\mathcal{A}}_{\rm C}$ may vary by a factor of 2–3 in the local interstellar medium (e.g., Zubko et al. 2004) and the mantle accretion rate, $\hat{D}$, depends linearly on this factor. With such an assumption, the initial conditions in cases of partial removal of carbon mantles are easily constructed just

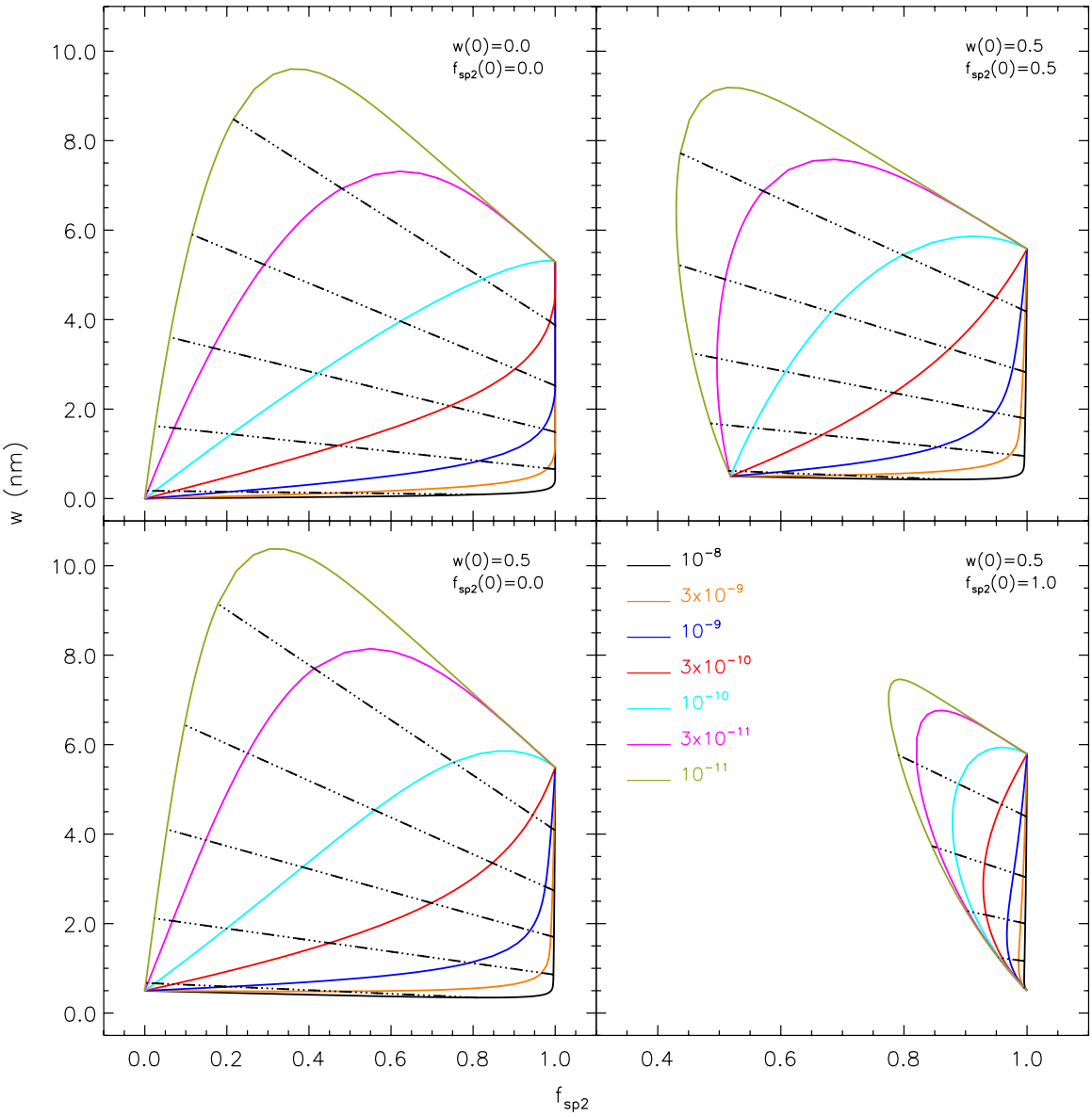

Figure 1. Theoretical distribution of mantle thickness w and normalized sp^2 mantle carbon fraction, $f_{sp^2} = \delta_{sp^2} x_{sp^2}/(\delta_{sp^2} x_{sp^2} + \delta_{sp^3} x_{sp^3})$. Evolutionary tracks are shown as solid lines starting from different initial conditions (see Equation (4)). (a) $(f_{sp^2}, w) = (0, 0)$; (b) (0,0.5); (c) (0.5,0.5); (d) (1,0.5). Each curve is labeled by the value of the scaled photo-darkening rate $s_{\rm pd}^{-1}$ in cm^3 K$^{-1/2}$ yr^{-1}. Dashed lines trace the iso-s curves.
(A color version of this figure is available in the online journal.)

deriving the fractional amount of carbon in the mantle leftover, x_w, and setting $x_{\rm C} = 1 - x_w$.

We remark that the expressions in Equation (4) are, strictly speaking, part of a much larger system of differential equations, which includes also the time-dependent chemical evolution model to which they are coupled. This is the reason why evolutionary tracks computed with the same value of $s_{\rm pd}$, but different initial conditions (i.e., curves of the same color in different panels of Figure 1) may intersect (and indeed some do). This does not contrast with the unicity of the solutions of a set of differential equations, because what intersects are not distinct, complete, many-dimensional solutions of the whole system (which indeed either never intersect or are entirely coincident), but rather their projections onto the much smaller $w - f_{sp^2}$ plane.

Finally, we estimate the asymptotic mantle thickness for a line of sight from the approximate analytic solutions derived in the Appendix, Equation (A1), with $x_{\rm C} \sim 0$

$$w \sim \frac{\hat{\mathcal{A}}_{\rm C}}{\langle \sigma_d n_d \rangle / [{\rm H}]} \times \left(\frac{\delta_{\rm C}}{m_{\rm C}} \right)^{-1} = 0.54 \times \left(\frac{\hat{\mathcal{A}}_{\rm C}/{\rm ppm}}{R_V} \right) \ {\rm nm}, \quad (5)$$

where we substitute $\langle \sigma_d n_d \rangle / [{\rm H}] \sim R_V / 5.9 \times 10^{21}$ cm^{-1}/[H] and $\delta_{\rm C} = \delta_{sp^2}$. Using $R_V = 3.1$ and $\hat{\mathcal{A}}_{\rm C} = 20$ ppm (the value for the average Galactic ISEC; Mulas et al. 2013), we find $w \sim 4$ nm (see Figure 1).

3. OBSERVATIONAL DATA

Mulas et al. (2013) recently performed a homogenous fit of all the Galactic extinction curves of the Fitzpatrick & Massa (2007) sample with a dust model, hereafter [CM]^2, consisting of spherical core-mantle dust particles, with a power-law size distribution, together with a "molecular" component,

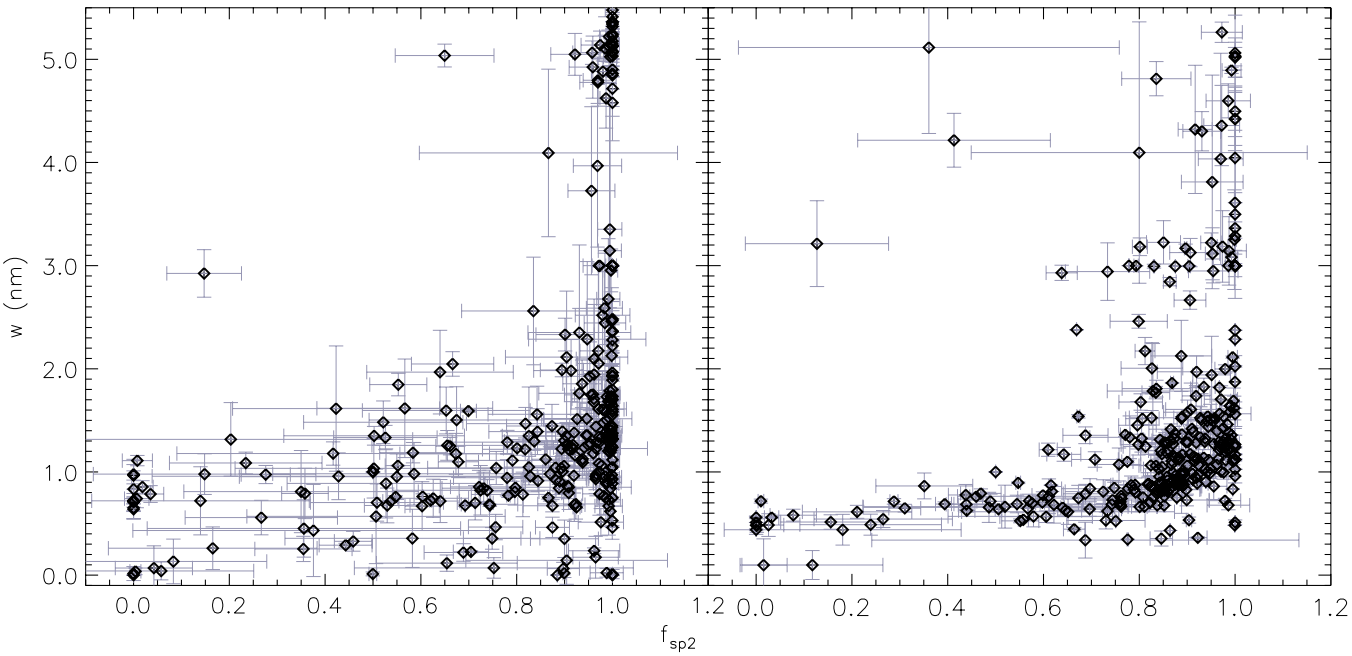

Figure 2. Observationally derived distribution of mantle thickness w and normalized sp^2 mantle carbon fraction ($\diamond$), with relative errors, for the simplified (left panel) and detailed (right panel) $[CM]^2$ models (Mulas et al. 2013).

i.e., PAHs, in their broad astronomical definition. PAHs are represented either by a superposition of actual, computed PAH photoabsorption cross sections (in the "detailed" $[CM]^2$ model) or by two Lorentzian profiles (in the "simplified" $[CM]^2$ model), representing the $\pi^* \leftarrow \pi$ and $\sigma^* \leftarrow \sigma$ resonances present in all aromatic moieties, be they free-flying molecules or nano-sized clusters. The classical dust grains are hollow silicate spheres covered by an internal sp^2 carbon layer and an outer sp^3 layer, in an idealized representation of the structure expected from the evolutionary model described in the previous section. The size distributions include distinct smaller and larger grain components, allowing for a gap in intermediate sizes.

Despite the apparent similarity, the simplified and detailed $[CM]^2$ models are qualitatively different: in the former, the two Lorentzian functions are independent, thereby allowing also for sp^3 carbonaceous nanoparticles, in which the $\pi^* \leftarrow \pi$ resonance is suppressed versus the $\sigma^* \leftarrow \sigma$ one; conversely, in the latter, for any combination of PAH cross sections the relative intensities of the two resonances can show only a modest variation due to charge state, but their spectral shapes can drift significantly away from Lorentzian profiles, due to differences in the detailed positions of bands in individual molecules. So, while both the simplified and the detailed $[CM]^2$ model fit equally well all ISECs, the molecular component of extinction has somewhat different degrees of freedom (reflecting different underlying physical assumptions), resulting also in different parameters for the classical component.

In both cases, from each fit one derives a carbonaceous mantle thickness w and ratio f_{sp^2} of thicknesses for the sp^2 versus sp^3 layers. From synthetic statistics in the fits, we also estimate uncertainties for both w and f_{sp^2} (see Mulas et al. 2013 for a detailed discussion of the methods employed).

Figure 2 displays w versus f_{sp^2}, as derived by Mulas et al. (2013) for the Fitzpatrick & Massa (2007) extinction curve sample. The left panel shows the results for the simplified $[CM]^2$ model and the right panel shows the results for the detailed one. The difference between the left and right panels of Figure 2 is remarkable: the left panel shows markedly more scatter, in particular in the left part of the plot where the evolutionary effects have more impact on the $f_{sp^2} - w$ distribution, while data points in the right panel appear to be more tightly constrained in a well-defined relatively small part of the $w - f_{sp^2}$ space. This difference stems from assuming, in the right panel, that the molecular component absorbs light as a collection of aromatic moieties, whereas in the left panel the $\pi^\star \leftarrow \pi$ and $\sigma^\star \leftarrow \sigma$ resonances are allowed to vary independently.

While Mulas et al. (2013) fit the extinction models solely using visible and ultraviolet extinction curves, the resulting models also yield the predicted extinction in the infrared, including the so-called aliphatic C–H stretch feature around 3.4 μm. Since the extinction in the infrared is much smaller than that in the ultraviolet, the ultraviolet extinction curve and the 3.4 μm feature are almost never observed for the same line of sight: lines of sight with a good measurement of the 3.4 μm feature are hardly observable in the ultraviolet and the 3.4 μm feature is hardly detectable in lines of sight with a well-determined ultraviolet extinction curve. We could find only one case among the lines of sight with extinction curves given by Fitzpatrick & Massa (2007), namely HD 204827, in which the aliphatic C–H stretch was detected. Figure 3 shows the observations from Valencic et al. (2003), with a superimposed extinction spectrum predicted by our extinction model, fit to the ultraviolet. Despite the very coarse sampling of the feature in the modeled extinction, dictated by the tabulated optical constants used in Mulas et al. (2013), the model and observations are in acceptable agreement. To ease visual comparison, on the same figure we also show superimposed the 3.4 μm feature measured on a laboratory sample by Mennella (2010), which best matches the interstellar feature. Perusing the extinction curves by Mulas et al. (2013), we find that the ratio equivalent width on A_V of the modeled 3.4 μm feature goes from zero to 5.2×10^{-4} μm mag^{-1}. If we use the laboratory profile to convert from equivalent width to maximum optical depth, this corresponds to $\tau_{\max} \simeq 4 \times 10^{-3}\,\mathrm{mag}^{-1}\,A_V$, encompassing the average interstellar value of $\sim 3.6 \times 10^{-3}\,\mathrm{mag}^{-1}\,A_V$ given by Gao et al. (2010).

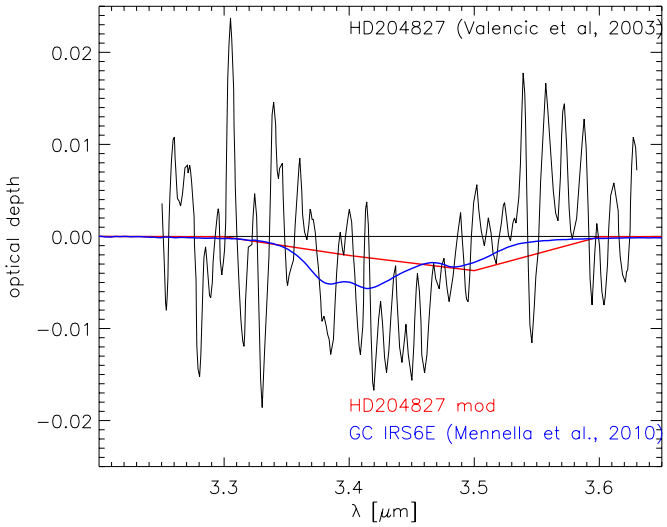

Figure 3. Optical depth of HD 204827 (Valencic et al. 2003), with the extinction spectrum predicted by our extinction model superimposed (red line) and a laboratory spectrum (Mennella 2010) known to provide an excellent fit to the band observed in GC IRS6E (Pendleton et al. 1994). The laboratory spectrum (blue line) was scaled to have the same integrated absorbance of the extinction model. The zero line is shown for easier comparison.

(A color version of this figure is available in the online journal.)

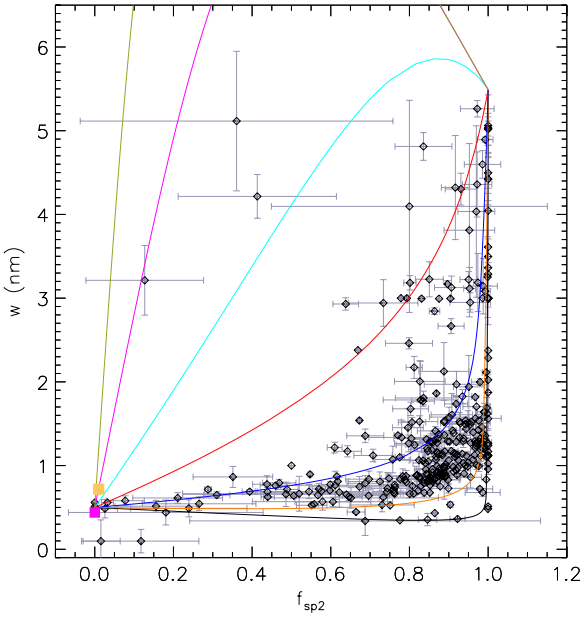

Figure 4. Comparison between observationally inferred (⋄) and modeled $w - f_{sp^2}$ couples (solid lines). Evolutionary tracks start from the initial conditions $(f_{sp^2}, w) = (0, 0.5)$. Lines with different colors refer to different values of the scaled photo-darkening rate (see Figure 1). The magenta square is the line of sight toward HD 62542 and the yellow square is the one toward HD 204827.

(A color version of this figure is available in the online journal.)

4. DISCUSSION: THE EVOLVING DUST

The observational results shown in the preceding sections have been obtained using a model consisting of a spherical void plus three concentric shells: silicate + hydrocarbon sp^2 + hydrocarbon sp^3. The relative fractions of these components and the thickness of the total carbon mantle are left to vary freely in response to the specifics of the fitting technique. The relative fractions of sp^2 and sp^3 bonding sites and the mantle thickness are also described by the evolutionary model summarized in Equation (4). Thus, it is possible to relate homologous, physically meaningful quantities derived from completely separate analyses. Such a comparison is shown in Figure 4, where we report the evolutionary tracks starting from the initial conditions $(f_{sp^2}, w) = (0, 0.5)$.

Data points obtained from the observations appear to follow rather closely the evolutionary tracks representing the evolution of carbonaceous mantles restarting from a thin leftover from a previous cycle, fully rehydrogenated. The vast majority of ISECs in Figure 4 are neatly bracketed by evolutionary tracks within a small range of values of the $s_{\rm pd}$ parameter, which happens to cover exactly the typical values assumed for the prevailing conditions in the diffuse interstellar medium. In particular, only two lines of sight appear to be unaccounted for by the choice of the initial conditions $(f_{sp^2}, w) = (0, 0.5)$. This suggests that typical recycling times in the interstellar medium should be shorter than the carbon mantle lifetimes. Lines of sight observationally known to traverse recently shocked interstellar material (e.g., by an expanding supernova shell) are expected to line up on the left side, i.e., carbonaceous mantles should be highly hydrogenated. This appears indeed to be the case for HD 62542 (Cardelli et al. 1990) and HD 204827 (Valencic et al. 2003, 2004), which are shown in Figure 4 by magenta and yellow squares, respectively. Interestingly, the 3.4 μm feature indicating an H-rich grain mantle has been observed toward HD 204827 (Valencic et al. 2003). Both lines of sight have a steep ultraviolet rise and a weak bump.

The parameters resulting from fitting ISECs with the detailed [CM]^2 model therefore turn out to be strikingly consistent with our evolutionary picture. We can think of no conceivable reason for the fitting procedure in Mulas et al. (2013) to produce such a distribution of points in the $w - f_{sp^2}$ plane as a random artifact, so we conclude it must be a real physical effect. Conversely, the simplified [CM]^2 model shows a much weaker consistency with some kind of function relation between w and f_{sp^2}. This means that the observed pattern comes out only as a result of assuming the molecular component to absorb light as a collection of aromatic manifolds. If the $\pi^* \leftarrow \pi$ and $\sigma^* \leftarrow \sigma$ resonances are allowed to vary independently, this deconstructs the physical coherence of the extinction model with respect to the evolution of dust grain mantles. This is consistent with the recent findings of Li & Draine (2012) and Yang et al. (2013) that carbonaceous nanoparticles small enough to be stochastically heated to emit in the mid-infrared must be almost entirely aromatic, with at most a very small aliphatic component.

In the framework of our evolutionary model, given an observational point in the $w - f_{sp^2}$ plane, we can invert the evolutionary curve it lies on to derive the corresponding $s_{\rm pd}$ and $s_{\rm ev}$, the evolutionary age. We can thereafter build a histogram of the distribution of $s_{\rm ev}$ values, which is shown in Figure 5. This was obtained using the data points from the detailed [CM]^2 model and inverting the evolutionary curves restarting from $w = 0.5$ nm and $f_{sp^2} = 0$, which were shown above to be most consistent with the assumed evolutionary model. This figure shows a broad maximum at $s_{\rm ev} \sim 10^9$ cm^{-3} K$^{1/2}$ yr. Assuming typical interstellar values for density, $n_{\rm H} \sim 100\,{\rm cm}^{-3}$, and kinetic temperature, $T_k \sim 100$ K, we find that the observed evolutionary ages of carbonaceous mantles peak at times of about a few million years. The resulting photo-darkening time (corresponding to the maximum density of data points in Figure 4) results in $t_{\rm pd} \sim 0.3$–$1 \times 10^6/\chi$ yr, in good agreement

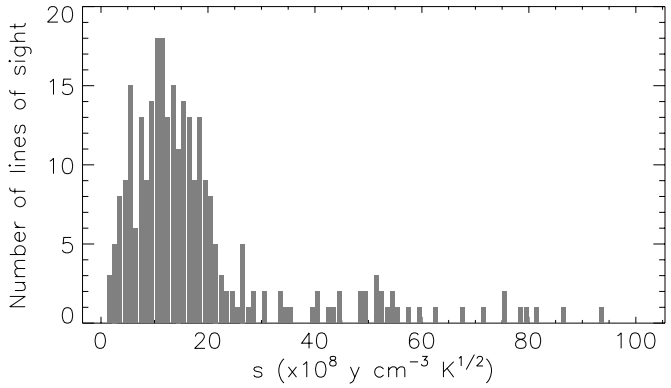

Figure 5. Distribution of the Galactic ISECs from the Fitzpatrick & Massa (2007) sample, as a function of the evolutionary indicator s_{ev}.

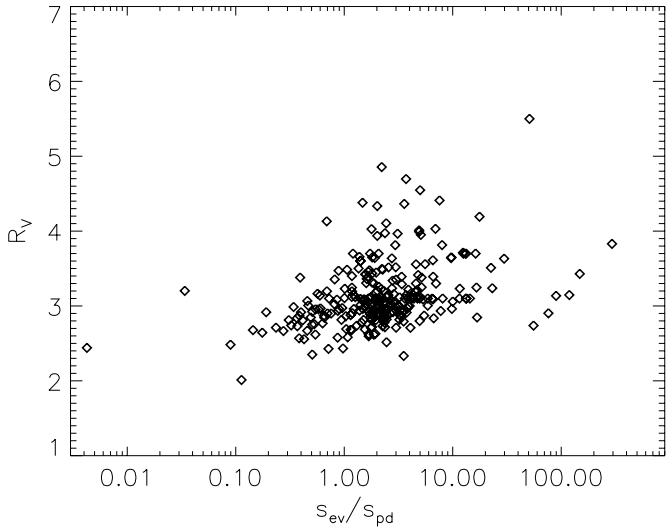

Figure 6. Relation between R_V and the carbon processing stage s_{ev}/s_{pd}.

with the results of laboratory experiments on amorphous carbon (e.g., Iida et al. 1984; Mennella et al. 2001). We note that the timescales over which dust evolves in clouds are comparable to the probable ages of clouds themselves. For either shorter or longer timescales, the extinction should vary in a predictable way. Hence, through the study of interstellar extinction, we may in principle be able to identify the evolutionary history of the diffuse clouds in the interstellar medium.

Lastly, we relate R_V, the ratio of total-to-selective extinction, to the evolutionary stage of carbon dust, as traced by the ratio between the evolutionary and photo-darkening times $s_{ev}/s_{pd} = \chi t/t_{pd}$ (Figure 6). The plot provides evidence for the existence of two roughly distinct regimes in which $s_{ev}/s_{pd} \lesssim 10$ and $s_{ev}/s_{pd} \gtrsim 100$. In Figure 6, we did not report those lines of sight with (scaled) photo-darkening times $s_{pd} \lesssim 10^7/\chi$ cm^{-3} K$^{1/2}$ yr (and thus their s_{ev}/s_{pd} are larger than 100). For these lines (approximately 20 in number), the values of $f_{sp^2} \sim 1$ and thus a precise assignment of s_{pd} is prevented; only an upper limit can be derived. This happens because of the asymptotic behavior of the evolutionary tracks, which all tend to become very close to the $f_{sp^2} = 1$ line in the $w - f_{sp^2}$ plane (see Figure 1).

In the region $s_{ev}/s_{pd} \lesssim 10$, where most of the lines of sight reside, the observationally derived R_V estimates tend to crowd about the fiducial value $R_V = 3$, when $t \approx t_{pd}/\chi$. On the contrary, for evolutionary times much larger than t_{pd}/χ, R_V values are dispersed and erratic. The same occurs to the values of mantle thicknesses that are scattered, but generally larger

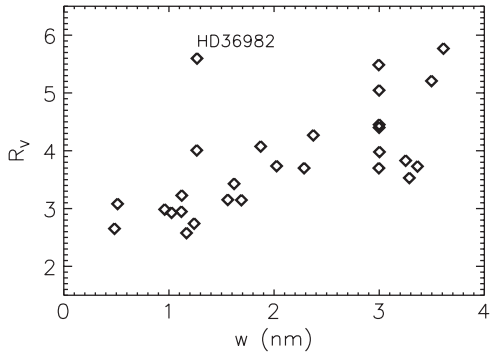

Figure 7. Relation between R_V and the carbon mantle thickness w for highly evolved ISECs, $s_{ev}/s_{pd} \gtrsim 100$.

than 1 nm. ISECs (in the light of the present model) are time dependent because of two factors: the gradual accumulation of carbon atoms on dust grains and the photo darkening of the resulting hydrocarbon mantle. As the mantle chemical composition reaches its final stage, the evolution of dust is driven by mantle accretion only, in which all grain sizes are modified simultaneously. Indeed, such a process appears to be imprinted in the ISECs for which $s_{ev}/s_{pd} \gtrsim 100$ (Figure 7): R_V and the mantle thickness w are related strongly with a moderate dispersion given by the effect of different size distributions. For such lines of sight, graphitization is driven by ultraviolet photolysis, but even other mechanisms such as, e.g., thermal annealing, may contribute to an increase in the concentration of sp^2 bonding sites.

The line of sight to HD 36982 is the one showing the largest departures from a linear relation $w - R_V$. HD 36982 is a sightline in which the relative amount of C and Si in grains is reduced compared with the Galactic averaged value. Barbaro et al. (2004) selected a sample of 41 lines of sight (including HD 36982) showing such a deficiency of metals incorporated in dust, 9 of which were part of the Fitzpatrick & Massa (2007) sample: 6 out 9 of these ISECs show a ratio $s_{ev}/s_{pd} \gtrsim 100$, while for one (HD 37061) the ratio is slightly larger than 10.

5. CONCLUSIONS

Cardelli et al. (1989) found that the shape of ultraviolet extinction curves correlates with the parameter $R_V = A_V/E(B-V)$, providing a link between one measure of dust grain environment and the wavelength dependence of the extinction. Thus, if the value of R_V can be determined from optical and infrared photometry, then the properties of the entire ultraviolet–infrared extinction curve can be predicted. However, while such a representation is very successful at describing ISECs as functions of few parameters, such parameters are not physically meaningful per se, but are complicated, largely unknown functions of the real physical quantities describing the interstellar material producing the extinction. The important question is how the variation of the extinction curve and its topological uniformity translate into the physical properties of dust grains. Infrared data suggest that the composition and the structure of carbonaceous dust vary within the interstellar medium and that these variations involve changes in the relative abundance of sp^2 and sp^3 hybridized bonded components (e.g., Pendleton & Allamandola 2002; Chiar et al. 2013). Similar variations are observed in laboratory samples of hydrogenated amorphous carbon (e.g., Duley & Hu 2012) due to changes in composition driven by factors such as hydrogen content, temperature, and ultraviolet photolysis. Such changes can be described through a photo-darkening

time, a change of the absorption edge that corresponds to a decrease of the optical gap, in agreement with the general result that hydrogen favors the sp^3 carbon hybridization and reduces the degree of aromatic sp^2 clusters in hydrogenated carbons (Robertson 1991). The characterization of dust extinction in terms of such chemical evolutionary factors is, of course, superimposed on other, mainly dynamical, processes such as grain size modulation in shocks. If the size distribution of grains was to be changed, then the extinction profile would also change. Still, the dispersion due to evolutionary regional factors is significant compared with that in the observational data (Cecchi-Pestellini et al. 2010).

We have developed here an evolutionary dust model, which was kept as simple as possible while still representing fairly accurately the processes described above, as they are expected to occur in the diffuse interstellar medium. The only free parameters of this model are essentially the scaled photodarkening time and the initial conditions, leaving very little room to adjust the model to match the observational data, as those obtained from Mulas et al. (2013). The distribution of observed ISECs in the $w - f_{sp^2}$ plane delineates a coherent evolutionary scenario for the Galactic dust. One free parameter, $s_{\rm pd}$, determines the evolutionary track with scaled time $s_{\rm ev}$ of carbonaceous dust mantles. Conversely, fitting any ISEC with the $[\mathrm{CM}]^2$ model observationally determines the mantle chemical composition and thickness.

In general, the agreement is extremely convincing, enabling us to draw some conclusions on the life cycle and properties of interstellar dust. In the framework of the $[\mathrm{CM}]^2$ model, comparison of the observationally determined data with evolutionary tracks shows the following points.

1. The establishment of a coherent evolutionary scenario for carbon dust requires a population of aromatic feature carriers.
2. Most of the ISECs in the Fitzpatrick & Massa (2007) sample correspond to dust mantles that restarted growing after being almost completely removed, with the leftover fully rehydrogenated, by, e.g., occasional shocks.
3. Most ISECs are on tracks with $3 \times 10^8 < s_{\rm pd} < 10^9$ cm^{-3} K$^{1/2}$ yr, where fluctuations (within a factor of three) are induced by regional differences in the strength of the interstellar ultraviolet radiation field (gas density and temperature are incorporated in the evolutionary variable s).
4. The evolutionary age of ISECs peaks at times of few Myr, assuming typical diffuse interstellar conditions, comparable to the probable average age of diffuse clouds, on the basis of statistical considerations.
5. $R_V \sim 3$ is reached when $s_{\rm ev} \approx s_{\rm pd}$; this result suggests that, in average, most lines of sight are left free to radiatively evolve for $t \sim 0.3$–1×10^6 $(100\,\mathrm{cm}^{-3}/n_{\rm H})$ $(100\,\mathrm{K}/T_{\rm k})^{1/2}$ yr.
6. About 10% of lines of sight are associated with photodarkening times shorter than the average Galactic value, suggesting the presence of very strong ultraviolet fields, and other forms of $sp^3 \rightarrow sp^2$ annealing.

Finally, we note that the present results might have implications on the global histories of dust grains. During their lifetime, dust grains cycle through several diffuse/dense phases (e.g., Li & Greenberg 1997). Assuming the total lifetime for a dust grain to be approximately a few hundred million years (Serra Díaz-Cano & Jones 2008), about the average age of a giant molecular cloud (Blitz & Williams 1999), and considering the latter to undergo a number of dense phases of the order of 10 (Sánchez & Parravano 1999), each with a lifespan of few times the free fall time, we derive a dust residence time in each phase of a few tens of millions of years. During a dense phase, dust grains are covered by an icy coating of volatiles, which protect the underlying carbon mantles, thereby "freezing" their chemical composition. During each cycle, little refractory material is expected to form from icy mantles and remain attached to the grain when the ice evaporates. Before and during the subsequent diffuse regime (which is the only one in which the ultraviolet extinction can be currently measured), the emerging dust collections may be subjected to shocks or, to a minor extent, left relatively undisturbed. Thus, the observationally inferred results shown in Figure 2 may incorporate the imprinting of "little aged" dust grains, sparsely populating the right portion of the diagram depicted in Figure 5. We shall explore this aspect in a subsequent publication.

Variations in interstellar ISECs along different lines of sight in the Milky Way Galaxy, and from one galaxy to another, are routinely interpreted as arising from changes in the relative abundances of the components that contribute to the extinction. In this work, we show that these variations can be related to differences in the local physical conditions through an evolutionary process in the interstellar gas. Then, ISECs could be a very useful tool for defining those physical conditions in the Milky Way or in other galaxies. A natural extension of this work will be its validation in environments markedly different from the interstellar medium of the solar neighborhood: physical situations in which the life cycle of the interstellar medium is known to be very different either globally, e.g., much more frequent shocks in starburst galaxies, or locally, because of independent observational constraints on individual lines of sight.

This research has been supported by the Autonomous Region of Sardinia, Project CRP 26666 (Regional Law 7/2007, Call 2010). A.Z. gratefully acknowledges the Sardinia Regional Government for the financial support of his PhD scholarship (P.O.R. Sardegna F.S.E. Operational Programme of the Autonomous Region of Sardinia (Italy), European Social Fund 2007-2013-Axis IV Human Resources, Objective l.3, Line of Activity l.3.1.). The authors thank the anonymous referee for comments and suggestions that improved the clarity of the paper.

APPENDIX

ANALYTIC APPROXIMATIONS

The equation coefficients in Equation (4) are weakly dependent on time, through the quantities $\langle \sigma_d n_d \rangle / [\mathrm{H}]$, derived integrating over the dust size distribution, as this changes in time during mantle accretion, and the mantle density $\delta_{\rm C}$. Setting both quantities to constant values, we obtain the approximate analytic solutions corresponding to initially bare silicate cores:

$$\begin{cases} x_{\rm C}(s) = \exp(-\hat{A} \times s) \\ x_{sp^3}(s) = \dfrac{\hat{A}}{\left(s_{\rm pd}^{-1} - \hat{A}\right)} \times \left[x_{\rm C}(s) - \exp\left(-s_{\rm pd}^{-1} \times s\right)\right] \\ w = \dfrac{\hat{D}}{\hat{A}\delta_{\rm C}} \left[1 - x_{\rm C}(s)\right]. \end{cases} \tag{A1}$$

For $s \to \infty$, the expressions in Equation (A1) give $x_C \to 0$, $x_{sp^3} \to 0$, $x_{sp^2} \to 1$, and $w \to \hat{D}/(\hat{A}\delta_C)$. Finally, when $s_{pd} \to \infty$, $x_{sp^2} \to 0$ and $x_{sp^3} \sim 1 - x_C$. Curves (Equation (A1)) with $s =$ const. are straight lines parallel to the $x_{sp^2}-$axis. Such a simple behavior is not shared by exact numerical solutions, i.e., iso-s curves are not straight lines when the analytical approximation ceases to be valid (see Figure 1).

REFERENCES

Barbaro, G., Geminale, A., Mazzei, P., & Congiu, E. 2004, MNRAS, 353, 760
Blitz, L., & Williams, J. P. 1999, in The Origin of Stars and Planetary Systems, ed. C. J. Lada & N. D. Kylafis (Dordrecht: Kluwer), 3
Cardelli, J. A., Clayton, G. C., & Mathis, J. S. 1989, ApJ, 345, 245
Cardelli, J. A., Suntzeff, N. B., Edgar, R. J., & Savage, B. D. 1990, ApJ, 362, 551
Casu, S., Cecchi-Pestellini, C., & Aiello, S. 2001, MNRAS, 325, 826
Cecchi-Pestellini, C., Cacciola, A., Iatì, M. A., et al. 2010, MNRAS, 408, 535
Cecchi-Pestellini, C., & Williams, D. A. 1998, MNRAS, 296, 414
Chiar, J. E., Tielens, A. G. G. M., Adamson, A. J., & Ricca, A. 2013, ApJ, 770, 78
Duley, W. W., & Hu, H. 2012, ApJ, 761, 115
Fitzpatrick, E. L., & Massa, D. 2007, ApJ, 663, 320
Gao, J., Jiang, B. W., & Li, A. 2010, E&PS, 62, 63
Greenberg, J. M. 1984, SciAm, 250, 124
Iatì, M. A., Saija, R., Borghese, F., et al. 2008, MNRAS, 384, 591
Iida, S., Ohtaki, T., & Seki, T. 1984, in AIP Conf. Proc. 120, Optical Effects in Amorphous Semiconductors, ed. P. C. Taylor & S G. Bishop (Melville, NY: AIP), 258
Jones, A. 2012a, A&A, 540, A1
Jones, A. 2012b, A&A, 540, A2, (erratum 545, C2 [2012])
Jones, A. P., Duley, W. W., & Williams, D. A. 1990, QJRAS, 31, 567
Jones, A. P., Fanciullo, L., Köhler, M., et al. 2013, A&A, 558, 62
Jones, A. P., Tielens, A. G. G. M., Hollenbach, D. J., & McKee, C. F. 1996, ApJ, 433, 797
Li, A., & Draine, B. T. 2012, ApJL, 760, L35
Li, A., & Greenberg, J. M. 1997, A&A, 323, 566
Maíz Apellániz, J., & Rubio, M. 2012, A&A, 541, A54
Mennella, V. 2010, ApJ, 718, 867
Mennella, V., Muñoz Caro, G. M., Ruiterkamp, R., et al. 2001, A&A, 367, 355
Mulas, G., Zonca, A., Casu, S., & Cecchi-Pestellini, C. 2013, ApJS, 207, 7
Pendleton, Y. J., & Allamandola, L. J. 2002, ApJS, 138, 75
Pendleton, Y. J., Sandford, S. A., Allamandola, L. J., Tielens, A. G. G. M., & Sellgren, K. 1994, ApJ, 437, 683
Robertson, J. 1991, Prog. Solid State Chem., 21, 199
Sánchez, D. N. M., & Parravano, A. 1999, ApJ, 510, 795
Serra Díaz-Cano, L., & Jones, A. P. 2008, A&A, 492, 127
Snow, T. P., & Witt, A. N. 1996, ApJL, 468, L65
Valencic, L. A., Clayton, G. C., & Gordon, K. D. 2004, ApJ, 616, 912
Valencic, L. A., Clayton, G. C., Gordon, K. D., & Smith, T. L. 2003, ApJ, 598, 369
Whittet, D. C. B. 2003, in Dust in the Galactic Environment (Bristol: Institute of Physics)
Woodall, J., Agúndez, M., Markwick-Kemper, A. J., & Millar, T. J. 2007, A&A, 466, 1197
Yang, X. J., Glaser, R., Li, A., & Zhong, J. X. 2013, ApJ, 776, 110
Zonca, A., Cecchi-Pestellini, C., Mulas, G., & Malloci, G. 2011, MNRAS, 410, 1932
Zubko, V., Dwek, E., & Arendt, G. 2004, ApJS, 152, 211